




**Alternating regimes of motion in a model with cell-cell interactions**Nara Guisoni <sup>1,\*</sup> Karina I. Mazzitello <sup>2,†</sup> and Luis Diambra <sup>3,‡</sup><sup>1</sup>*Instituto de Investigaciones Fisicoquímicas Teóricas y Aplicadas, Universidad Nacional de La Plata, CONICET, 1900 La Plata, Buenos Aires, Argentina*<sup>2</sup>*Instituto de Investigaciones Científicas y Tecnológicas en Electrónica, Universidad Nacional de Mar del Plata, CONICET, B7608 Mar del Plata, Buenos Aires, Argentina*<sup>3</sup>*Centro Regional de Estudios Genómicos, Universidad Nacional de La Plata, CONICET, 1900 La Plata, Buenos Aires, Argentina*

(Received 30 December 2019; accepted 26 May 2020; published 11 June 2020)

Cellular movement is a complex dynamic process, resulting from the interaction of multiple elements at the intra- and extracellular levels. This epiphenomenon presents a variety of behaviors, which can include normal and anomalous diffusion or collective migration. In some cases, cells can get neighborhood information through chemical or mechanical cues. A unified understanding about how such information can influence the dynamics of cell movement is still lacking. In order to improve our comprehension of cell migration we have considered a cellular Potts model where cells move actively in the direction of a driving field. The intensity of this driving field is constant, while its orientation can evolve according to two alternative dynamics based on the Ornstein-Uhlenbeck process. In one case, the next orientation of the driving field depends on the previous direction of the field. In the other case, the direction update considers the mean orientation performed by the cell in previous steps. Thus, the latter update rule mimics the ability of cells to perceive the environment, avoiding obstacles and thus increasing the cellular displacement. Different cell densities are considered to reveal the effect of cell-cell interactions. Our results indicate that both dynamics introduce temporal and spatial correlations in cell velocity in a friction-coefficient and cell-density-dependent manner. Furthermore, we observe alternating regimes in the mean-square displacement, with normal and anomalous diffusion. The crossovers between diffusive and directed motion regimes are strongly affected by both the driving field dynamics and cell-cell interactions. In this sense, when cell polarization update grants information about the previous cellular displacement, the duration of the diffusive regime decreases, particularly in high-density cultures.

DOI: [10.1103/PhysRevE.101.062408](https://doi.org/10.1103/PhysRevE.101.062408)**I. INTRODUCTION**

Cell motion plays a key role in many physiological processes including tissue morphogenesis, wound healing, and immune and inflammatory response. It is known that the movement of cells is strongly influenced by cell-cell interactions, which grants a wide spectrum of behaviors. Cell motion can be categorized in terms of its external environment, which can present directional asymmetry in response to a chemical stimulus, or be isotropic, without a preferred direction. In this sense, the single-cell tracking technique provides substantial evidence that in the absence of chemotactic cues, cells perform a persistent random walk, which has been modeled by the Ornstein-Uhlenbeck (OU) process [1]. In the case of directional asymmetry of the environment, the cell is said to perform taxis and cell movement has been widely modeled using the Keller-Segel diffusion equation [2]. In addition to this categorization, cell motion can refer to the movement of individual cells with or without neighbors [3,4] or to a cell population acting as an aggregate [5–7].

Experimental results focused on individual movements present characteristics of Brownian particles [8,9]: exponential decay of the velocity autocorrelation function (ACF) and linear growth with time of the mean-square displacement (MSD), the latter at large timescales [10]. These features can be explained by the OU process or, equivalently, the conventional Klein-Kramers description [1,11]. However, there exist cell motions without chemotaxis that do not follow the OU process. For example, movements of epithelial cells and aggregates of *Hydra* cells were reported as anomalous diffusion processes [5]. Also human fibroblasts and keratinocytes move in a manner that contradicts the OU process [5]. Similarly, Takagi *et al.* reported different cell movement behaviors with anomalous diffusion for *Dictyostelium* cells in different physiological conditions [12]. These experiments fit well with a generalized Langevin model which includes a memory kernel for cell velocity [13]. Furthermore, long-term analysis of Madin-Darby canine kidney cells has revealed a superdiffusive behavior, in the absence of external cues [4,14]. These findings can be explained by the fractional Klein-Kramers equation [4] and highlight that cell movement contains a more complex dynamics than the persistent random walk. The fractional Klein-Kramers equation can be considered as a phenomenological approach, able to describe anomalous diffusion in terms of very general physical mechanisms. However, it is rather limited when it comes to indicating

\*naraguisoni@gmail.com

†kmazzite@gmail.com

‡ldiambra@gmail.com

which biological ingredients lead to an anomalous behavior. Thus, alternative modeling that allows one to get biological insight through testing different hypotheses becomes really interesting.

On the other hand, anomalous dynamics have also been observed in the collective movement of self-propelled particles in complex media [15–18]. Examples of such active entities in chemical and biological systems are colloidal nanorods [19], chemotactic movement in the presence of obstacles [20], and also colloidal particles driven by an external field [21].

Over the past few decades, the cellular Potts model (CPM) [22] has been successfully extended to study active cell movement [6,23–27]. Recently, we introduced a cell reorientation model based on the CPM framework [28]. In this model, cell movement is governed by a driving field whose direction changes following a discrete version of the OU process. In contrast, previous models for noninteracting particles have applied the OU process on the velocity vector, leading to white-noise fluctuations on the direction angle [8,9,29,30]. It is known that when the orientation angle fluctuates without correlations (i.e., in the absence of the friction term) the system exhibits Brownian motion [29,31]. However, when the friction term is present, we found that high-density cultures exhibited a double exponential for the velocity ACF, in contrast to an exponential characterizing the Brownian motion of low-density cultures. For both densities the MSD behaves as a persistent random walk for the short timescale studied in [28]. On the other hand, at long timescales the proposed cell reorientation dynamic leads the system to a ballistic regime. A crossover from a diffusive to a ballistic regime has been reported in the case of models of noninteracting particles [29,30]. However, the influence of cell-cell interactions on this crossover is poorly understood.

In this work we are interested in studying the effect of cell-cell interactions on alternating regimes of motion occurring in a large timescale. In this sense, we use the CPM with active cell movement, with two types of dynamics for the cell orientation angle as introduced in [28]. First, we consider a “naive” angle actualization where the new orientation is related to the field direction operating in the previous step, regardless of the cellular direction of displacement. In the second case, the update direction depends on the mean orientation performed by the cell in the previous steps. This implementation of the field direction update grants a sort of feedback mechanism, because at each time step the angle of the driving field is influenced by the recent cell history, taking into account that cell interactions can lead to blocking or deviation of the original cell trajectory. We have studied how the crossover from the diffusive to the ballistic regime is affected both by the neighborhood information gathered by the cell in previous displacements and by different cell densities. In addition, we have calculated the temporal and spatial correlations of cell velocity, the average distance traveled by a cell during the time interval in which the driving field is constant, and the angle direction of cell displacement.

## II. MODEL

The CPM is a modified Potts model which includes different terms of energy that make it able to reproduce some

biophysical properties of cells such as deformations of cell membrane, adhesion, and motility in an excluded-volume manner. In the model, at each site of the lattice a spin  $\sigma_i = 1, \dots, Q$  is assigned and cells are represented by domains with the same spin; thereby if  $\sigma_i = M$ , with  $1 \leq M \leq Q$ , it belongs to the cell labeled  $M$ . The dynamics of the model are governed by the Hamiltonian, or energy function, which guides cell behavior by distinguishing the low-energy configurations (or favorable) from the high-energy ones. The Hamiltonian consists of a term corresponding to the sum of all surface energies, which represent cell-cell adhesion properties. In addition, to prevent cells from breaking or disappearing, additional terms related to cell area and perimeter are needed in the Hamiltonian. Thus, the energy function considered here is given by

$$H_0 = \sum_{i,j \text{ neighbors}} J_{\sigma_i \sigma_j} (1 - \delta_{\sigma_i \sigma_j}) + \sum_{M=1}^Q \kappa (V_M - V_0)^2 + \sum_{M=1}^Q \Gamma (L_M - L_0)^2, \quad (1)$$

where  $\delta_{\sigma_i \sigma_j}$  is the Kronecker delta and the first sum is over all neighboring site pairs, representing the boundary energy of the interacting cells. The second and third terms in Eq. (1) correspond to the energy costs when cell volume and perimeter deviate from the target values  $V_0$  and  $L_0$ , respectively. In addition, cells interact with a medium which has spin variable  $\sigma_i = 0$ , with no target area or perimeter. The adhesion constant between different cells is denoted by  $J_{\text{cell-cell}}$  and between cells and medium is  $J_{\text{cell-medium}}$ . Further, to consider cell motility preferentially along the direction of a driving field  $\vec{F}$ , an additional term should be added to the Hamiltonian (1) [23,28], as we will see below.

The system evolves using Monte Carlo dynamics. The variation of energy in a proposed trial configuration is given by

$$\Delta H = \Delta H_0 + \sum_{M=1}^Q \vec{F}_M \cdot \Delta \vec{r}_M, \quad (2)$$

where  $\Delta H_0$  is the change of energy related to Eq. (1),  $\vec{r}_M$  denotes the displacement of the center of cell  $M$ , and  $\vec{F}_M$  is the driving field acting on cell  $M$ . The acceptance, or not, of a new configuration is given by the Metropolis prescription (see [28] for details). The unit of time, a Monte Carlo step (MCS), is defined as  $N$  trials of movement, with  $N$  the number of spins in the lattice.

The driving field is characterized by a direction denoted by  $\Theta$  and an intensity  $F$ . We consider that the intensity  $F$  is constant over time and has the same value for all cells. However, the direction of the driving field operating over cell  $M$ ,  $\Theta_M$ , is actualized according to the OU process,  $d\Theta_M(t) = -\lambda \Theta_M(t) dt + \sigma dW(t)$ , where  $\lambda$  is the friction coefficient ( $0 \leq \lambda < 1$ ),  $\sigma$  determines the magnitude of the fluctuations, and  $dW(t)$  represents the Wiener process. For our Monte Carlo simulations, it is necessary to use a discrete version of this stochastic differential equation, which can be identified with a first-order autoregressive process as

$$\Theta_M(n) = (1 - \lambda)\Theta_M(n-1) + \sigma \epsilon(n), \quad n = 1, 2, \dots, (3)$$

where  $\epsilon(n)$  is a white noise with zero mean and unit variance ( $\sigma_\epsilon^2 = 1$ ) and  $n$  is the discrete time;  $\lambda$  and  $\sigma$  were defined previously.

Note that it is not mandatory that the cell displacement has the same direction as the associated driving field, since both cell-cell interactions and stochastic fluctuations can deviate the cell from the driving field direction. Thus, the angle of the driving field  $\Theta_M$  is not necessarily equal to the angle direction of the cell movement, which will be denoted by  $\alpha_M$ . If the previous direction of the cell displacement is considered in the actualization of the driving angle, we have positive feedback which mimics the situation in which the cell produces its own chemotactic signal. This aspect was taken into account previously by other authors in Potts-like models [6,27,32]. In that way, Kabla considers that the motile force is oriented along the mean velocity of the cell over its past time steps, without friction or noise [27]. For Szabó *et al.* [6] the change in cell polarization is proportional to a spontaneous decay with respect to its previous value and a reinforcement of the cell displacement direction during the time step considered. We propose an alternative update rule to the angle of the driving field  $\Theta_M$  which considers a feedback mechanism

$$\Theta_M(n) = (1 - \lambda)\overline{\alpha}_M(n-1) + \sigma\epsilon(n), \quad (4)$$

where  $\overline{\alpha}_M(n-1)$  is the mean displacement angle over the previous  $\tau$  MCSs and  $\lambda$  and  $\sigma$  were defined previously. Equation (4) represents positive feedback since the actualization of  $\Theta_M$  reinforces the previous cell direction. Differently from previous formulations [6,27,32], our proposal for the feedback actualization rule takes into account fluctuations. In addition, an advantage of Eq. (4) is the possibility of a direct comparison with Eq. (3): The only difference between them is the dependence on the mean cell polarity  $\overline{\alpha}_M$  instead of on the previous direction of the driving field  $\Theta_M$ .

When using Eq. (3) the new angle direction of the driving field is related to the previous direction of the driving field, regardless of the angle direction of cell displacement. For that reason, we call Eq. (3) a naive OU model. For both actualization procedures, the initial direction of the cell  $M$ ,  $\Theta_M(0)$ , is chosen randomly between  $[0, 2\pi]$ ;  $\Theta_M$  evolves independently of the field operating in other cells. The updating time in Eqs. (3) and (4),  $n$ , is different from the time of actualization of cell configurations. In particular, at each time step the direction of the driving field for each cell  $M$  changes with probability  $1/\tau$  according to Eq. (3) or (4). Thus, the change in the directions  $\Theta_M$  and  $\alpha_M$  occurs at a mean time  $\tau$  independently of the direction of other cells.

The dynamic process underlying both Eqs. (3) and (4) determines a distribution of cell direction centered at  $\Theta = 0$  for  $\lambda \neq 0$ . The width of  $\Theta$  distribution depends on the parameters  $\lambda$  and  $\sigma$ . Consequently, at long timescales, a directed random walk is expected [33].

### III. RESULTS

For all simulations in this paper, we use the fixed parameter values  $J_{\text{cell-cell}} = 0.1$ ,  $J_{\text{cell-medium}} = 0.01$ ,  $\Gamma = 0.2$ ,  $\kappa = 1$ ,  $\sigma = \pi/3$ ,  $F = 10$ ,  $T = 2$ , and  $\tau = 10$  MCSs. In order to use physically meaningful units, we considered the units of time and distance as  $\tau$  and the average diameter of the cells

( $d = 16$  pixels [28]), respectively. We use throughout the paper different values for the friction coefficient  $\lambda$ . We use periodic boundary conditions and a square lattice of  $1024 \times 1024$  sites. The model dynamics does not present evident lattice-size effects. In fact, identical results were obtained by using lattice sizes of  $256 \times 256$  and  $512 \times 512$  sites. The density  $\rho$  is defined as the ratio between the area occupied by the cells and the medium. In this way, we calculate the number of spins with  $\sigma_i \neq 0$  related to the total number of spins, since the medium is identified by  $\sigma_i = 0$ . Low- and high-density simulations correspond to  $\rho = 0.2$  and  $0.9$ , respectively. The total numbers of cells for low- and high-density simulations are  $Q = 819$  and  $3686$ , respectively (for the lattice size used). More details about initial conditions and thermalization can be found in [28]. Cell velocity is defined as  $\vec{v}_M(t) = (v_x^M, v_y^M) = \Delta\vec{r}_M(t)/\Delta t$ , where  $\Delta\vec{r}_M(t) = \vec{r}_M(t + \Delta t) - \vec{r}_M(t)$  and  $\Delta t = 1$  MCS. The direction of the cell movement is computed as  $\alpha_M = \arctan(v_y^M/v_x^M)$ .

In order to characterize the movement of a cell population we calculate the mean-square displacement as  $\text{MSD}(t) = \langle [\vec{r}_M(t) - \vec{r}_M(0)]^2 \rangle$ , where the calculation is made for each cell  $M$  between the starting point at  $t = 0$  and the actual position at time  $t$  and the average is taken over all  $Q$  cells of the simulation by means of a simple average. According to Fig. 1, the MSD presents two or three regimes in the timescale considered, depending on the value of  $\lambda$  and on the updating rule used. For  $\lambda = 0.01$  and the OU actualization (3), we can see that at short times the MSD is almost ballistic and after that it resembles a random walk, regardless of the density. For the other situations, the MSD has three regimes: It is almost ballistic at short times, diffusive at intermediate timescales, and ballistic at long times. When the direction of the driving field is actualized by using the OU process with feedback (4), the crossover between the random-walk behavior and the ballistic regime at long times occurs for  $\lambda = 0.10$  before it does for  $0.01$ . On the other hand, when the OU actualization is used, this crossover is present for  $\lambda = 0.10$  but not for  $0.01$ . Consequently, the duration of the diffusive period is shorter when the friction coefficient is higher (same actualization model and different values of  $\lambda$ ) and when the feedback is present (same value of  $\lambda$  and different actualization models). In order to understand these results, we turn to discuss the meaning of the different regimes observed for the MSD along the different timescales. For all cases, the almost ballistic short-time behavior is related to the persistence time of the driving force,  $\tau$ . In fact, in a previous paper [28] we showed that the temporal behavior of the MSD scales with  $\tau$  for the OU actualization. The diffusive behavior of the MSD, also present for all cases shown in Fig. 1, is the result of the fluctuations in the direction of the driving field, since Eqs. (3) and (4) are stochastic equations. However, the actualization of  $\Theta$  is not completely random. In fact, the friction coefficient  $\lambda$  introduces correlations in the successive directions of cell displacement, leading to a biased distribution of cell direction. The effect of this bias is observed at long times in the ballistic asymptotic behavior. In addition, when using Eq. (4) the presence of feedback in the angle direction actualization raises correlations and therefore anticipates the ballistic regime. In addition, from Fig. 1 we see that the MSD obtained from the angle updating rule with feedback is greater than or equal

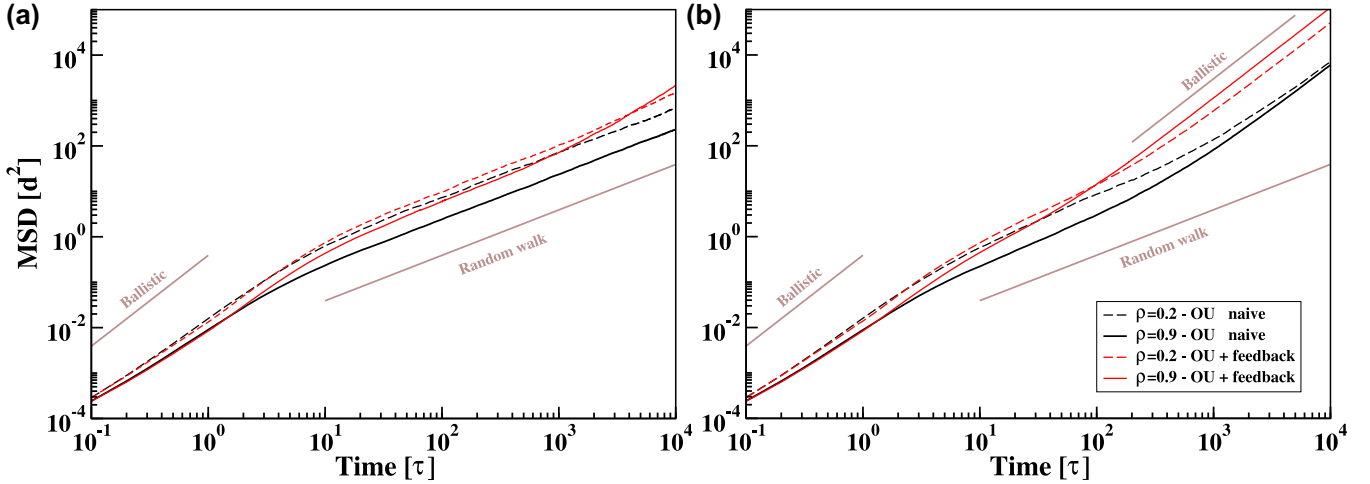


FIG. 1. A log-log plot of the mean-square displacement versus time (distance in units of average cell diameter  $d$  and time in units of  $\tau$ ). The direction of the driving field is actualized according to the Ornstein-Uhlenbeck process (OU naive) and the Ornstein-Uhlenbeck process with feedback (OU + feedback) for (a)  $\lambda = 0.01$  and (b)  $\lambda = 0.10$ , with  $\rho = 0.2$  (dashed line) and  $\rho = 0.9$  (solid line). Lines with slopes equal to 2 (ballistic) and 1 (random walk) are shown for comparison purposes only. The MSD is calculated between the starting point at  $t = 0$  and the actual positions at time  $t$  and averaged over all  $Q$  cells of the simulation. More details are given in the text.

to that found with the OU actualization. This result suggests that feedback helps cells avoid collisions with other cells, making the movement more effective. Finally, we discuss the effect of density on the MSD, starting with the model of OU actualization. Low-density configurations have MSD higher than or equal to that obtained for high density, for both values of  $\lambda$  (see the black lines in Fig. 1). In fact, a lower MSD for high-density cultures is expected, since crowded cell cultures usually disturb the movement of cells. The same behavior related to density can be observed at short and intermediate times when the feedback updating rule is used. However, at long times, the high-density culture presents higher MSD than the low-density one, for  $\lambda = 0.10$  and feedback update. This inversion in the MSD suggests that the feedback gives rise to a spatially coordinated movement of cells in high-density simulations.

The time behavior of the MSD shown in Fig. 1 suggests the potential of a scaling. As noted previously, the MSD presents three regimes and therefore two different crossovers. The first time crossover  $t_{c1}$  separates the almost ballistic regime at short times from diffusive behavior at an intermediate timescale and only depends linearly on  $\tau$  [28]. This is because the driving field acting on cells changes in the average time  $\tau$ . Thus, cells perform a ballistic movement for this limited time. The second time crossover  $t_{c2}$ , from which MSD grows ballistically at long times, strongly depends on the friction coefficient  $\lambda$ . We found that the second time crossover behaves as  $t_{c2} \sim \lambda^{-h}$ , in units of  $\tau$ , for a given cell density and updating rule. The MSD data collapse is achieved in two steps [34]. Considering first the OU model for low-density cultures, every curve of the MSD versus time corresponding to a given value of  $\lambda$  in the inset of Fig. 2(a) is rigidly translated to move the first crossover point to the origin, by rescaling the vertical  $y$  axis as  $\text{MSD}/ct^\beta$  and the horizontal  $x$  axis as  $t/t_{c1}$ , with the first time crossover equal to a constant value  $t_{c1} = 9$  in units of  $\tau$ . Then the vertical  $y$  axis is rescaled by  $\gamma = 1/\ln[\text{MSD}(t_{c2})] =$

$1/\ln(a\lambda^{-h})$  and the horizontal  $x$  axis by  $\chi = 1/\ln(t_{c2}/t_{c1})$ . A last transformation (a backward rotation  $y \rightarrow ycx^\beta$ ) is included in order to recover the overall behavior of the MSD. The resulting plot is shown in Fig. 2(a) for the MSD data of the inset. The very good collapse on a single curve is apparent and gives support to the idea of universality of the MSD for the OU model for low-density cultures. However, this scaling law fails for high densities [see Fig. 2(b)]. Clear differences among the curves for different values of the friction coefficient  $\lambda$  in the region of diffusive behavior are observed. This indicates that cell-cell interactions affect the MSD in an unpredictable manner. The same qualitative results were found for the OU model with feedback given by Eq. (4) (not shown here). In this case, MSD curves associated with low-density cultures collapse with the same scaling of the OU naive model, but with different constant values. In the case of high-density cultures the collapse is not found, evidencing once again the effect produced by cellular interactions.

The temporal behavior of MSD scales with time as  $\text{MSD}(t) \sim t^{\beta(t)}$ , where the exponent  $\beta$  characterizes the different regimes observed. In that way, a ballistic behavior is associated with  $\beta = 2$ , whereas normal diffusion presents  $\beta = 1$ . The logarithmic derivative of the MSD allows the calculation of  $\beta$  as  $\beta(t) = \frac{d \ln \text{MSD}(t)}{d \ln(t)}$ . Similar measurements were used to study cell migration [4] and intracellular transport [35] in both experiments and models and in a simple model that mimics the diffusion of a particle in an anisotropic amorphous material [15]. Figure 3 shows the behavior of  $\beta$  as obtained from the two angle updating rules, for low (dashed lines) and high (solid lines) densities and different values of  $\lambda$ . Further,  $\beta$  was calculated by linear interpolation of the MSD curves in the log-log plane. We used a time-sliding window, the size of which increases exponentially with the temporal scale. At the short timescale the exponent  $\beta$  corresponds to anomalous diffusion. At this scale, we can note that for the OU actualization low-density cultures present greater values

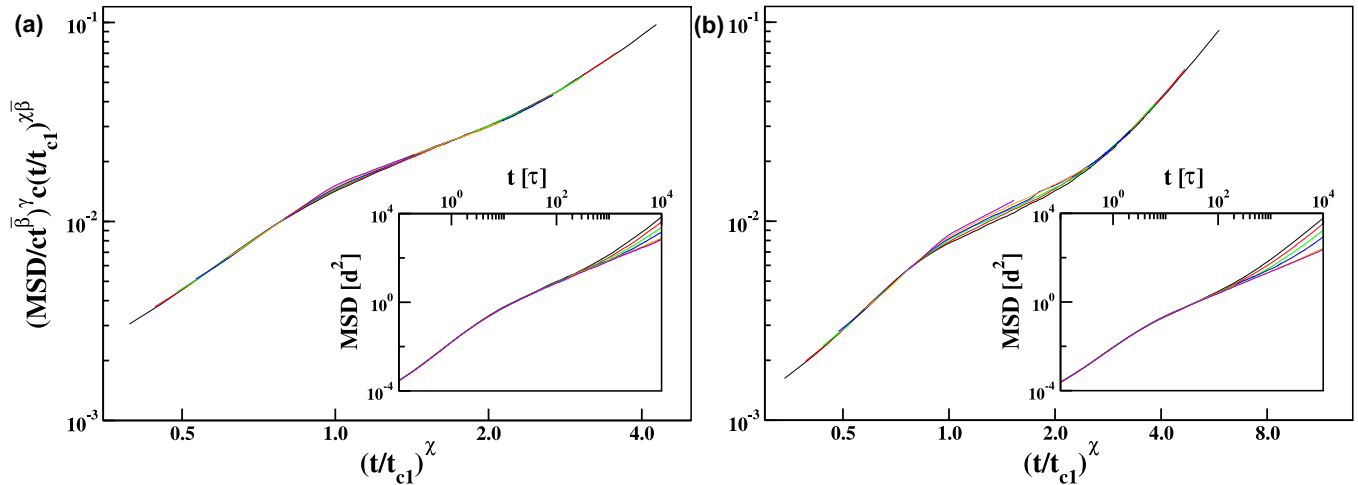


FIG. 2. Rescaled MSD of the curves of the inset, for results obtained from OU naive actualization model at (a) low and (b) high cell density. Scaling functions are defined as  $\gamma = 1/\ln[\text{MSD}(t_{c2})] = 1/\ln(a\lambda^{-h})$  and  $\chi = 1/\ln(t_{c2}/t_{c1})$ , with constant values (a)  $a = 3.0 \times 10^{-5}$ ,  $h = 6.4$ ,  $t_{c1} = 9$  (units of  $\tau$ ),  $t_{c2} = 4.04 \times 10^{-4}\lambda^{-h}$  (units of  $\tau$ ),  $c = 0.015$ , and  $\bar{\beta} = 1.8$  and (b)  $a = 3.5 \times 10^{-5}$ ,  $h = 5.6$ ,  $t_{c1} = 8$  (units of  $\tau$ ),  $t_{c2} = 1.26 \times 10^{-3}\lambda^{-h}$  (units of  $\tau$ ),  $c = 0.0086$ , and  $\bar{\beta} = 1.6$ . The insets correspond to the log-log plot of the MSD versus time (distance in units of average cell diameter  $d$  and time in units of  $\tau$ ), for results obtained from the OU naive actualization model at (a) low and (b) high cell density. The curves correspond to different values of the friction coefficient:  $\lambda = 0.01, 0.05, 0.07, 0.08, 0.09, 0.10$  (violet, orange, blue, green, red, and black, respectively).

of  $\beta$  than high-density ones. This aspect is less evident when the feedback mechanism is considered, since  $\beta$  for low- and high-density cultures presents almost the same value in the range [3, 10] in  $\tau$  units. In addition, at short timescale a slight increase in  $\beta$  for the update with feedback can be observed. These results indicate that feedback makes cell movement more efficient, particularly for high-density cultures, as discussed before. At an intermediate timescale,  $\beta$  decreases and the MSD tends to exhibit a diffusive behavior. In particular, for the OU actualization and low- $\lambda$  values, the diffusive behavior

is observed at intermediate and long timescales. For the other conditions of Fig. 3, the transition between short-time and long-time ballistic regimes is so tight that the exponent  $\beta = 1$  is almost not reached, but it will be referred to as a diffusive regime. The duration of the diffusive regime decreases with  $\lambda$  (for the same angle updating rule) and with the feedback (for the same value of  $\lambda$ ), as pointed out in Fig. 1. Also, for the OU actualization and low- $\lambda$  values,  $\beta$  is independent of the density at intermediate and long timescales. For the other conditions in the same timescales, the high-density

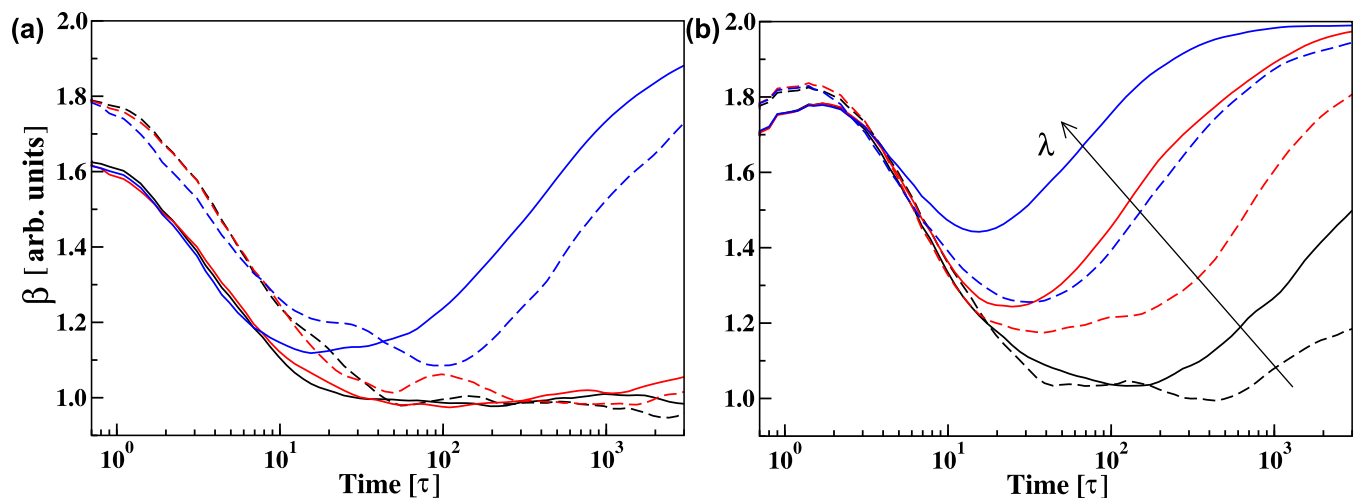


FIG. 3. Logarithmic derivative of the MSD  $\beta(t)$  versus time (in units of  $\tau$ ), calculated from data shown in Fig. 1 and additional data. The direction of the driving field is actualized according to (a) the OU naive process and (b) the OU process with feedback for different values of  $\lambda = 0.01, 0.05, 0.10$  (dark, red, and blue, respectively) and  $\rho = 0.2, 0.9$  (dashed and solid lines, respectively). We used a time-sliding window, the size of which depends on time. Successive measurements of  $\beta$  are made in the time interval  $[[1.775^k], [1.775^{(k+4)}]]$  in time units of MCSs, with  $k = 1, 1.2, 1.4, \dots, 16$ , since the MSD data are considered until  $t = 10^5$  MCSs. Here  $[\dots]$  indicates the greatest integer less than or equal to the argument.

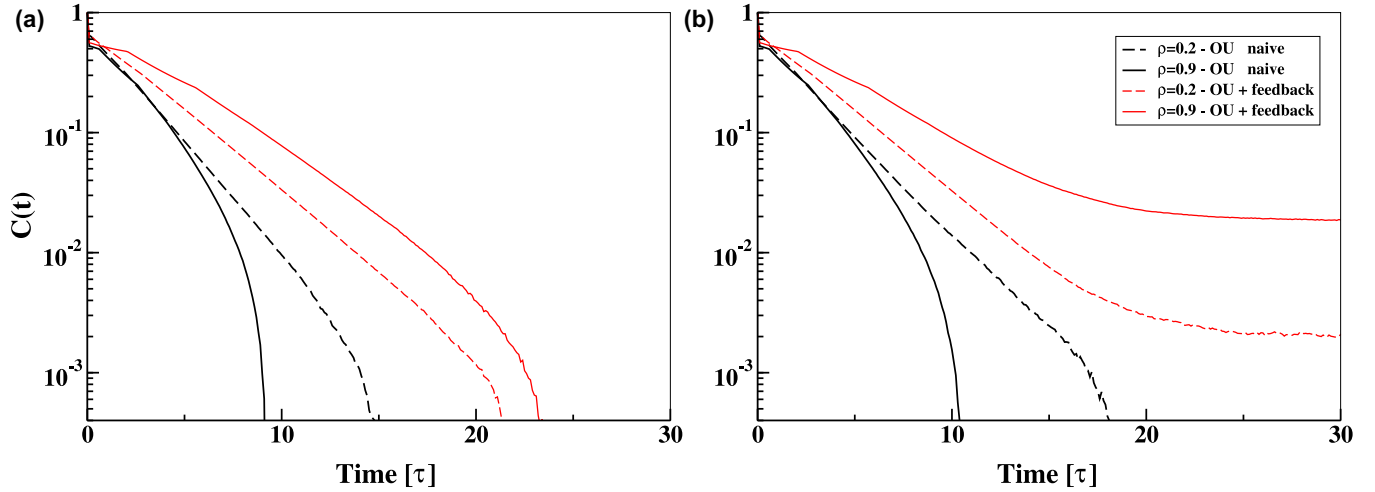


FIG. 4. Semilogarithmic plot of the velocity ACF function  $C(t)$  versus time (in units of  $\tau$ ). The direction of the driving field is actualized according to the OU naive process and the OU process with feedback, for different densities  $\rho = 0.2, 0.9$  (dashed and solid lines, respectively) and friction coefficients (a)  $\lambda = 0.01$  and (b)  $\lambda = 0.05$ . Here  $C(t)$  was averaged over all  $Q$  cells of the simulation and over  $t_0$  for each simulation sample. We consider three samples for  $\rho = 0.2$  and one for  $\rho = 0.9$ , each with  $6 \times 10^4$  MCSs. More details are given in the text.

cultures present greater values of  $\beta$  than low-density ones. In addition, from the behavior of  $\beta$  at long timescales when the feedback is considered [Fig. 3(b)], we can suppose that for a larger timescale (that is, for  $t \geq 10^4\tau$ )  $\beta$  will continue to increase until it reaches  $\beta = 2$ . In fact, we can expect the same behavior for Fig. 3(a), since for both actualization rules there is a preferential direction for cell movement at long times. As we have discussed previously, the correlation comes from the friction term and it is reinforced by the feedback. Cell-cell interactions also increase correlations at intermediate and long timescales.

The ACF velocity is another important tool to characterize cell movement [36]. For one cell the velocity ACF is defined as  $C_M(t) = Z_M(t)/Z_M(0)$ , where  $Z_M(t) = \frac{1}{T-t} \sum_{t_0=1}^{T-t} [\vec{v}_M(t_0 + t) \cdot \vec{v}_M(t_0)]$ , with  $T$  the total duration of the simulation. The velocity ACF of the simulation  $C(t)$  is obtained by a simple average of  $C_M(t)$  over the total number of cells  $Q$ . In addition, in order to improve statistics it is possible to make an ensemble average by considering several independent simulations that are averaged through a simple mean. Figure 4 shows that the velocity ACF obtained for the angle updating rule with feedback (4) is always higher than the one obtained for the naive angle update (3), regardless of the values of  $\lambda$  or  $\rho$ . In fact, if cells are more successful in avoiding collisions with other cells we expect a higher ACF. In Fig. 4, for the OU actualization, high-density cultures have smaller ACF than low-density cultures, for both  $\lambda = 0.01$  and  $0.05$ . This result can be understood by the fact that a crowded neighborhood usually disrupts the movement of cells. However, when the feedback update is considered, this relation is inverted: High-density cultures have a greater value of ACF than low-density ones, independently of the value of  $\lambda$ . Therefore, we can conclude that the feedback makes cell movement more efficient, mostly for high-density cultures. Actually, when the update with feedback is used in high-density cultures there is a competition between two effects: On the one hand, a crowded environment hinders cell movement while, on the other, the

feedback promotes it. In the OU update only the first effect can be found. Because of that, the difference in the velocity ACF between the two update rules is more evident for high-density cultures.

Also, Fig. 4 shows that the ACF is greater for  $\lambda = 0.05$  than for  $\lambda = 0.01$ , regardless of the density or the update model. This result indicates that the friction coefficient enhances the correlation in cell movement, as discussed before. Finally, for the OU process with a feedback update and  $\lambda = 0.05$  the ACF presents a very slow decrease at long times, consistent with an algebraic decay, independently of the density. For the other parameters considered in Fig. 4 the ACF drops to zero before  $t = 25$  in units of  $\tau$ .

The spatial correlations of the cell velocities are also used to study cell movement. The spatial correlation for a time  $t$  is calculated as  $C^t(r) = \frac{1}{N_{\text{pairs}}} \sum_{M, M'}^* \vec{v}_M \cdot \vec{v}_{M'} / (|\vec{v}_M| |\vec{v}_{M'}|)$ , where  $r = |\vec{r}_M - \vec{r}_{M'}|$  is the distance between the center of mass of cells  $M$  and  $M'$ . Here  $\sum^*$  runs over all cells pairs  $M, M'$  that are at a distance  $r$  at time  $t$  and  $N_{\text{pairs}}$  is the total number of these pairs. The spatial correlation  $C(r)$  is obtained by means of a simple average of  $C^t(r)$  over all time steps. When comparing the two angle-update rules, we can see from Fig. 5 that  $C(r)$  is always higher when the update rule with feedback is used, as it is also the case for the ACF (Fig. 4). As discussed in a previous work [28], the peak close to the typical diameter of the cell ( $r = 1$  in units of  $d$ ) is related to anticorrelated velocities of cells that travel in opposite directions. At intermediate and long distances ( $r \gtrsim 1$  in units of  $d$ ), cells in high-density configurations are more correlated for both actualization rules and  $\lambda$  values. Apart from this,  $C(r)$  in high-density simulations approaches zero very slowly, as  $r$  increases, in particular for  $\lambda = 0.10$  and when using the feedback-update rule [Fig. 5(b)]. These results indicate that cell-cell contact induces long-range spatial correlation of cell velocity and that this effect is enhanced by both the feedback and the friction coefficient. Also, the difference in  $C(r)$  between low- and high-density cultures is more noticeable in

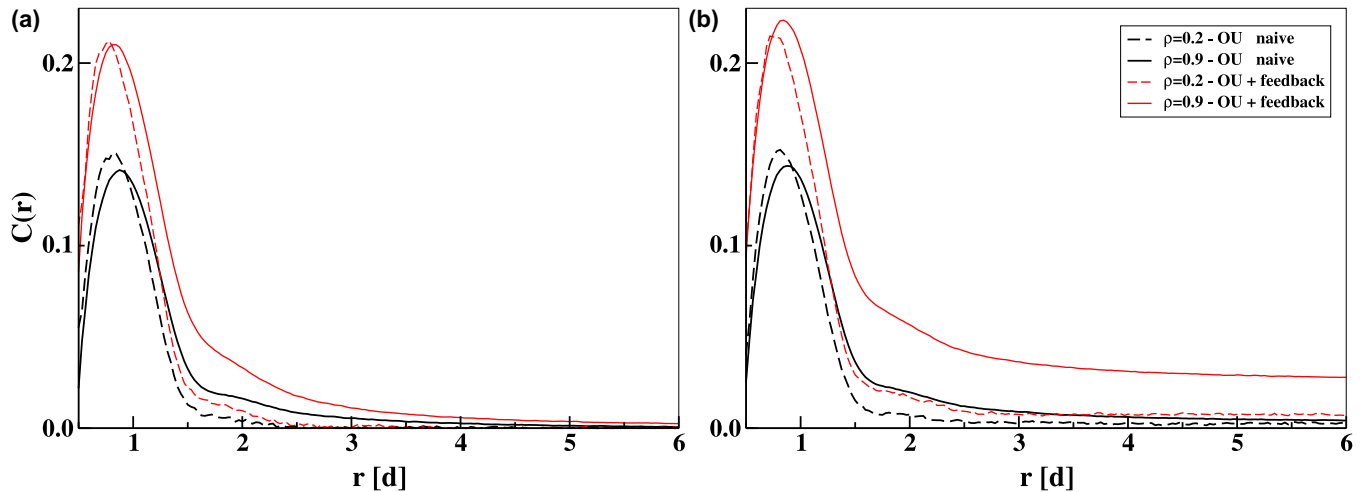


FIG. 5. Spatial correlation function of the velocities  $C(r)$  as a function of the distance  $r$  between cell pairs (in units of average cell diameter  $d$ ). The direction of the driving field is actualized according to the OU naive process and the OU process with feedback, for different densities  $\rho = 0.2, 0.9$  (dashed and solid lines, respectively) and friction coefficients (a)  $\lambda = 0.01$  and (b)  $\lambda = 0.10$ . Here  $C(r)$  is averaged over all cells of the simulation and over time until  $t = 10^5$  MCSs. More details are given in the text.

the case of update with feedback. Therefore, the effect of the feedback raising spatial correlations is greater for the crowded cultures, as observed for the temporal correlations in Fig. 4. These results might indicate a coordinated movement of cells in high-density cultures as a consequence of the feedback mechanism.

In order to get insight into the effect of the feedback mechanism and of different densities on cell movement, we introduce  $\bar{D}$ . We define the average distance  $\bar{D}$  traveled by a cell during the time interval in which the driving field is operating in a given direction. Mathematically, it is defined as

$$\bar{D} = \frac{1}{Q} \sum_{M=1}^Q \langle |\Delta \vec{r}_M(t_f - t_i)| \rangle_{I_t}, \quad (5)$$

where  $\Delta \vec{r}_M(t_f - t_i)$  is the cell displacement from the time the driving field starts operating,  $t_i$ , until the time of the next direction change,  $t_f$  (with  $t_f - t_i \sim \tau$ ). Here  $\langle \dots \rangle_{I_t}$  indicates the average over all time intervals  $I_t = [t_i, t_f]$ , that is, we consider all time intervals in which the driving field is operating in a given direction during the simulation run. Finally, the sum runs over all cells on the substrate. This magnitude gives information about the cell movement only in the short timescale ( $\sim \tau$ , i.e., during the first almost ballistic regime). For that reason  $\bar{D}$  presents similar values for different  $\lambda$  values, as we can see in Fig. 6(a). Further, it is expected that cells can move much more in low-density cultures than in a crowded medium, which is also evident in Fig. 6(a), where  $\bar{D}$  is much higher for  $\rho = 0.2$  than for  $\rho = 0.9$ . Figure 6(a) also establishes a comparison of the magnitude  $\bar{D}$  for the two angle-updating rules specified by Eqs. (3) and (4). In all cases, the average distance  $\bar{D}$  reached by the cells when the OU process with feedback is acting is greater than when the OU update is applied. In particular, we observe that in the case of a crowded medium there is a remarkable increment (of about 20%) of  $\bar{D}$  when the update with feedback is applied with respect to the OU actualization. For the low-density case

the increase is only about 3%. These results suggest that the OU process with feedback update promotes or increases cell displacement, especially in crowded environments.

By calculating the direction of cell movement  $\alpha_M$  for all  $Q$  cells during a certain simulation time, it is possible to obtain the histogram of  $\alpha$ , whose analysis allows us to study the existence of a preferred angle in cell movement. In Figs. 6(b)–6(e) we compare the two update rules given by Eqs. (3) and (4) for different situations: low and high densities and different values of  $\lambda$ . The bias observed in the angle distribution is more evident for higher values of  $\lambda$ , as shown in Figs. 6(b) and 6(c). This result is quite expected since the updating rules have a direction centered at  $\Theta = 0$  (for  $\lambda \neq 0$ ) that leads to directed motion at long timescales. However, the effect of cell-cell interactions is, *a priori*, more elusive. In this sense, we find that cell interactions increase the bias in cell movement, which is more evident when the feedback-update rule is acting. These results are in agreement with the fact that the ballistic regime occurs previously for the update rule (4) and for a more crowded environment, as seen in Figs. 1 and 3.

#### IV. DISCUSSION AND CONCLUSION

Much of the work about cell motility is based on the study of the time behavior of the second moment, the MSD. A system is considered to exhibit Brownian motion when the MSD increases linearly in time. Otherwise it is considered to present anomalous diffusion. However, we usually want to know more about the cell trajectories rather than only the second moment [3,4]. Other features of interest are the distribution and correlations of cell velocity. Thus, if normal diffusion occurs, the velocity correlation decreases to zero exponentially, or more quickly, while anomalous diffusion presents a slower ACF velocity decay. The MSD and the correlations can be theoretically derived only from simplified models [13,29,30,35,37]. This modeling feature is particularly interesting to get insight into the asymptotic behavior of the

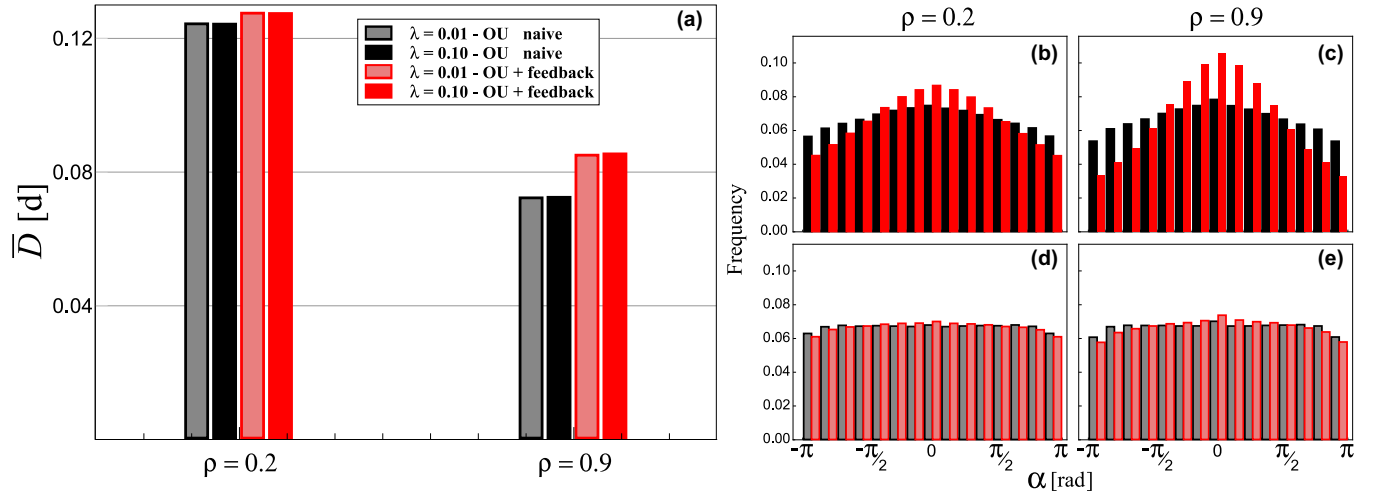


FIG. 6. (a) Average distance traveled by a cell during the time interval that the driving field is operating,  $\bar{D}$  (in units of average cell diameter  $d$ ), for densities  $\rho = 0.2$  and  $0.9$ . The direction of the driving field is actualized according to the OU naive process and the OU process with feedback (black and red, respectively) with friction coefficients  $\lambda = 0.01$  and  $0.10$  (different color patterns, as indicated). Histograms of the direction of the cell movement  $\alpha$  are shown for different conditions: (b)  $\rho = 0.2$  and  $\lambda = 0.10$ , (c)  $\rho = 0.9$  and  $\lambda = 0.10$ , (d)  $\rho = 0.2$  and  $\lambda = 0.01$ , and (e)  $\rho = 0.9$  and  $\lambda = 0.01$ . The update of the direction of the driving field is according to labels in (a). Here  $\bar{D}$  is averaged over all  $Q$  cells in the simulations until  $10^5$  MCSs (the first 500 MCSs are disregarded). In addition,  $\alpha$  was calculated for simulations until  $5 \times 10^4$  MCSs for  $\rho = 0.2$  and  $10^4$  MCSs for  $\rho = 0.9$ , in order to have similar quantity of data, that is,  $Q$  times the number of time steps. Error bars are smaller than the line thickness.

MSD. On the other hand, for models which include biological ingredients like cell volume and cell-cell interactions, such as the CPM-based ones, it is difficult to get analytical expressions. However, these models can add valuable information about cell motion [6,27,28,38]. For example, they are able to test feedback mechanisms from the neighborhood at a distinct spatial scale in an excluded-volume schema [27,38]. In addition, Kabla studied different cell dynamics for the collective movement resulting from the balance between adhesion and cell motile forces [27]. Here we have studied cell movement at long timescales addressing the effect of cell-cell interactions and neighborhood information gathered by the cell within the framework of a CPM-based model. We have considered that cells move actively according to a driving field that has a constant intensity and whose orientation is governed by two alternative OU updating rules.

We observed alternating regimes between ballistic and Brownian motion for the MSD. The almost ballistic behavior at short times is related to the persistence time  $\tau$  of the driving field [28]. At intermediate-time intervals the MSD becomes diffusive due to the random actualization of cell direction. A crossover from a quadratic to a linear regime in the MSD has been previously reported. In fact, in a model of self-propelled particles this transition is found when the diffusive behavior arising from particle reorientation dominates the persistence process [30]. In addition, when the OU dynamics is applied to update the particle velocities vector (instead of updating the angle direction as was done here) the same crossover is observed in the MSD and the resulting asymptotic regime is Brownian [1,29]. In addition to this initial crossing of regimes, we found a second crossover between the diffusive behavior and a ballistic regime at large timescales. The asymptotic ballistic regime is a consequence of the existence of a preferential direction in the angle-update

rule. This preferential direction is more evident for higher friction coefficients  $\lambda$ . Therefore, the second crossover occurs previously for large- $\lambda$  values. Furthermore, we show that this crossover also depends on the angle-update rule used, occurring earlier when Eq. (4) is operating. This result agrees with the fact that temporal and spatial correlations are higher when the update rule with feedback is used. In the same way, we observed that the feedback-update rule helps cells avoid collision against other cells, making the movement more effective along the preferential direction and therefore anticipating the ballistic regime. Finally, the transition to the long-term ballistic regime depends on cell-cell interactions and occurs previously in crowded cultures. In conclusion, we have shown that the appearance of the long-time ballistic regime is favored by the friction term  $\lambda$ , by the feedback updating rule, and also by a crowded environment. All these factors introduce correlations in cell movement, anticipating the crossover time between the diffusive and the ballistic regime. We also expect this crossover to be affected by  $\sigma$ , since greater values of  $\sigma$  are related to a more stochastic cell movement and should correspond to a longer diffusive period. Our findings might be related to previous results provided by a directed-random-walk model [33]. In this paper the time of appearance of the asymptotic ballistic regime depends on an anisotropy parameter, which fixes the correlations in the displacement direction: At higher values of this parameter (or stronger anisotropy), there is more correlation and the ballistic regime appears earlier [33].

The crossover between the diffusive and the ballistic regime at large timescales could be relevant in the context of the cell migration in tissues with a chemotactic gradient. For example, real-time cell tracking in intact thymic lobes has revealed that the thymocytes exhibit random-walk migration, but after positive selection they display a directed



motion [39,40]. Long-time cell tracking in tissues is difficult to access and in most cases experimental results refer to transient regimes [3,4,12,41]. For this reason, a direct comparison with theoretical models should be carefully carried out.

## ACKNOWLEDGMENTS

We acknowledge financial support from the Argentinian Science Agencies CONICET (Projects No. PIP 0597 and No. PIP 0681) and ANPCyT and from Universidad Nacional de La Plata.

- [1] G. E. Uhlenbeck and L. S. Ornstein, On the theory of the Brownian motion, *Phys. Rev.* **36**, 823 (1930).
- [2] E. F. Keller and L. A. Segel, Initiation of slime mold aggregation viewed as an instability, *J. Theor. Biol.* **26**, 399 (1970).
- [3] L. L. Li, S. F. Nørrelykke, and E. C. Cox, Persistent cell motion in the absence of external signals: A search strategy for eukaryotic cells, *PLoS ONE* **3**, e2093 (2008).
- [4] P. Dieterich, R. Klages, R. Preuss, and A. Schwab, Anomalous dynamics of cell migration, *Proc. Natl. Acad. Sci. USA* **105**, 459 (2008).
- [5] A. Upadhyaya, J.-P. Rieu, J. A. Glazier, and Y. Sawada, Anomalous diffusion and non-Gaussian velocity distribution of Hydra cells in cellular aggregates, *Physica A* **293**, 549 (2001).
- [6] A. Szabó, R. Ünnp, E. Méhes, W. O. Twal, W. S. Argraves, Y. Cao, and A. Czirók, Collective cell motion in endothelial monolayers, *Phys. Biol.* **7**, 046007 (2010).
- [7] A. Czirók, K. Varga, E. Méhes, and A. Szabó, Collective cell streams in epithelial monolayers depend on cell adhesion, *New J. Phys.* **15**, 075006 (2013).
- [8] C. L. Stokes, D. A. Lauffenburger, and S. K. Williams, Migration of individual microvessel endothelial cells: Stochastic model and parameter measurement, *J. Cell Sci.* **99**, 419 (1991).
- [9] G. A. Dunn and A. F. Brown, A unified approach to analyzing cell motility, *J. Cell Sci. Suppl.* **8**, 81 (1987).
- [10] R. Fürth, Die Brownsche bewegung bei berücksichtigung einer persistenz der bewegungsrichtung. Mit anwendungen auf die bewegung lebender infusorien, *Z. Physik* **2**, 244 (1920).
- [11] H. Risken, *The Fokker-Planck Equation: Method of Solution and Applications* (Springer, New York, 1989).
- [12] H. Takagi, M. J. Sato, T. Yanagida, and M. Ueda, Functional analysis of spontaneous cell movement under different physiological conditions, *PLoS ONE* **3**, e2648 (2008).
- [13] D. Selmeczi, S. Mosler, P. H. Hagedorn, N. B. Larsen, and H. Flyvbjerg, Cell motility as persistent random motion: Theories from experiments, *Biophys. J.* **89**, 912 (2005).
- [14] L. Diambra, L. C. Cintra, Q. Chen, D. Schubert, and L. da F. Costa, Cell adhesion protein decreases cell motion: Statistical characterization of locomotion activity, *Physica A* **365**, 481 (2006).
- [15] S. Bustingorry, E. R. Reyes, and M. O. Cáceres, Biased diffusion in anisotropic disordered systems, *Phys. Rev. E* **62**, 7664 (2000).
- [16] P. Romanczuk, M. Bär, W. Ebeling, B. Lindner, and L. Schimansky-Geier, Active Brownian particles: From individual to collective stochastic dynamics, *Eur. Phys. J. Spec. Top.* **202**, 1 (2012).
- [17] O. Chepizhko and F. Peruani, Diffusion, Subdiffusion, and Trapping of Active Particles in Heterogeneous Media, *Phys. Rev. Lett.* **111**, 160604 (2013).
- [18] O. Chepizhko, E. G. Altmann, and F. Peruani, Optimal Noise Maximizes Collective Motion in Heterogeneous Media, *Phys. Rev. Lett.* **110**, 238101 (2013).
- [19] D. Campos and V. Méndez, Superdiffusive-like motion of colloidal nanorods, *J. Chem. Phys.* **130**, 134711 (2009).
- [20] R. Grima, Directed cell migration in the presence of obstacles, *Theor. Biol. Med. Model.* **4**, 2 (2007).
- [21] J. P. Segovia-Gutiérrez, M. A. Escobedo-Sánchez, E. Sarmiento-Gómez, and S. U. Egelhaaf, Diffusion of anisotropic particles in random energy landscapes-an experimental study, *Front. Phys.* **7**, 224 (2020).
- [22] F. Graner and J. A. Glazier, Simulation of Biological Cell Sorting Using a Two-Dimensional Extended Potts Model, *Phys. Rev. Lett.* **69**, 2013 (1992).
- [23] N. J. Savill and P. Hogeweg, Modelling Morphogenesis: From single cells to crawling slugs, *J. Theor. Biol.* **184**, 229 (1997).
- [24] A. Maree, Modelling Dictyostelium discoideum Morphogenesis: The Culmination, *Bull. Math. Biol.* **64**, 327 (2002).
- [25] J. Käfer, P. Hogeweg, and A. F. M. Marée, Moving forward moving backward: Directional sorting of chemotactic cells due to size and adhesion differences, *PLoS Comput. Biol.* **2**, e0056 (2006).
- [26] A. F. M. Marée, V. A. Grieneisen, and P. Hogeweg, *The Cellular Potts Model and Biophysical Properties of Cells, Tissues and Morphogenesis* (Birkhäuser, Basel, 2007), pp. 107–136.
- [27] A. J. Kabla, Collective cell migration: Leadership, invasion and segregation, *J. R. Soc. Interface* **9**, 3268 (2012).
- [28] N. Guisoni, K. I. Mazzitello, and L. Diambra, Modeling active cell movement with the Potts model, *Front. Phys.* **6**, 61 (2018).
- [29] D. Campos, V. Méndez, and I. Llopis, Persistent random motion: Uncovering cell migration dynamics, *J. Theor. Biol.* **267**, 526 (2010).
- [30] F. Peruani and L. Morelli, Self-Propelled Particles with Fluctuating Speed and Direction of Motion in Two Dimensions, *Phys. Rev. Lett.* **99**, 010602 (2007).
- [31] C. Tojo and P. Argyrakis, Correlated random walk in continuous space, *Phys. Rev. E* **54**, 58 (1996).
- [32] J. B. Belmont, A. F. M. Marée, J. N. Lynch, M. J. Miller, and R. J. de Boer, Lymph node topology dictates T cell migration behavior, *J. Exp. Med.* **204**, 771 (2007).
- [33] S.-Y. Huang, X.-W. Zou, and Z.-Z. Jin, Directed random walks in continuous space, *Phys. Rev. E* **65**, 052105 (2002).
- [34] K. I. Mazzitello, L. M. Delgado, and J. L. Iguain, Low-coverage heteroepitaxial growth with interfacial mixing, *J. Stat. Mech.* (2015) P01015.
- [35] L. Bruno, V. Levi, M. Brunstein, and M. A. Despósito, Transition to superdiffusive behavior in intracellular actin-based transport mediated by molecular motors, *Phys. Rev. E* **80**, 011912 (2009).
- [36] J. P. Rieu, A. Upadhyaya, J. A. Glazier, N. B. Ouchi, and Y. Sawada, Diffusion and deformations of single hydra cells in cellular aggregates, *Biophys. J.* **79**, 1903 (2000).
- [37] M. A. Despósito, C. Pallavicini, V. Levi, and L. Bruno, Active transport in complex media: Relationship between

- persistence and superdiffusion, *Physica A* **390**, 1026 (2011).
- [38] C. P. Beatrici and L. G. Brunnet, Cell sorting based on motility differences, *Phys. Rev. E* **84**, 031927 (2011).
- [39] C. M. Witt, S. Raychaudhuri, B. Schaefer, A. K. Chakraborty, and E. A. Robey, Directed migration of positively selected thymocytes visualized in real time, *PLoS Biol.* **3**, e160 (2005).
- [40] E. J. Banigan, T. H. Harris, D. A. Christian, C. A. Hunter, and A. J. Liu, Heterogeneous CD8<sup>+</sup> T cell migration in the lymph node in the absence of inflammation revealed by quantitative migration analysis, *PLoS Comput. Biol.* **11**, e1004058 (2015).
- [41] J. B. Beltman, A. F. M. Marée, and R. J. de Boer, Analysing immune cell migration, *Nat. Rev. Immun.* **9**, 789 (2009).